# Phase Behavior of Pure Diblocks and Binary Diblock Blends of Poly(ethylene)−Poly(ethylethylene)

**Jin Zhao, Biswaroop Majumdar, Mark F. Schulz, and Frank S. Bates***

*Department of Chemical Engineering and Materials Science, University of Minnesota, Minneapolis, Minnesota 55455*

**Kristoffer Almdal and Kell Mortensen**

*Risø National Laboratory, DK-4000 Roskilde, Denmark*

**Damian A. Hajduk† and Sol M. Gruner**

*Department of Physics, P.O. Box 708, Princeton University, Princeton, New Jersey 08544-0708*

*Received May 26, 1995; Revised Manuscript Received November 7, 1995*⊗

ABSTRACT: We have determined the phase behavior of a series of model poly(ethylene)−poly(ethylethylene) (PE−PEE) diblock copolymers with poly(ethylene) block volume fractions ($f_{PE}$) ranging from 0.25 to 0.46. Four ordered microstructures make contact with the ODT: spheres arranged on a body-centered cubic lattice ($Im\bar{3}m$ space group), cylinders packed on a hexagonal lattice, a bicontinuous structure of space group $Ia\bar{3}d$, and lamellae. A fifth ordered phase, tentatively identified as hexagonally perforated layers (HPL), separates the cylindrical and lamellar morphologies at moderate or greater degrees of segregation. Binary blends of $f_{PE} = 0.37$ and 0.46 diblocks were used to investigate the bicontinuous cubic phase region in greater detail; these experiments indicate that this phase extends as much as 100 °C below the ODT for $\langle f_{PE} \rangle$ values in the blend from 0.385 to 0.420.

## I. Introduction

Block copolymer phase behavior has attracted intense interest for over three decades. Nevertheless, recent experimental and theoretical studies demonstrate that our understanding of this field is far from complete. Even the simplest architecture, diblocks, continues to yield surprising complexity, with two new ordered microstructures, hexagonally perforated layers (HPL)[1−5] and a bicontinuous cubic structure known as $Ia\bar{3}d$/gyroid*,[3,6,7] having recently been identified. (The evidence for a previously established structure, the ordered bicontinuous double diamond, or OBDD,[8,9] has been called into question within the past year.[10]) Multiblock copolymers containing three or more chains arranged in linear,[11,12] star, and branched[13] configurations have produced a variety of other unanticipated and intriguing microstructures.

Our research group has focused on neat diblock copolymer melts in an effort to identify aspects of phase behavior near the order−disorder transition (ODT). We have prepared a large number of model hydrocarbon compounds and employed small-angle neutron and X-ray scattering (SANS/SAXS), dynamic mechanical spectroscopy (DMS), and transmission electron microscopy (TEM) in characterizing the conditions that lead to various ordered states. A summary of these results for four chemically distinct pure diblock systems has been published.[14] The four diagrams presented in that work resemble one another in their large-scale structural features such as the general succession of phases observed with decreasing minority component volume fraction ($f$) and the approximate locations of the phase boundaries separating the various ordered structures. When our data are examined at higher resolution, however, notable differences in phase behavior become apparent. We expect that careful evaluation of these differences and correlation of these shifts with other physical or chemical properties of the polymers will prove significant in enhancing our understanding of the factors that stabilize ordered morphologies in block copolymer melts. Unfortunately, our ability to establish phase behavior in detail is hampered by the necessity of synthesizing a new sample for each target composition. Aside from the sheer burden of conducting sufficient polymerizations, the precision required to resolve increasingly finer features in composition and molecular weight becomes intractable.

Blends of two or more well-characterized diblock materials offer an attractive solution to this difficulty. Such a blend may behave as a single-component material with a minority component volume fraction approximately equal to that determined by the composition of the original diblocks and their proportions in the blend. However, the extra degree of freedom provided by the second component in the blend has a number of implications for the phase behavior of the system. First, macroscopic phase separation may occur, resulting in the appearance of coexisting microstructures of differing sizes[15] or space groups. Second, local segregation of blocks might also occur inside the unit cells of nonlamellar morphologies, resulting in the stabilization of these structures and a consequent shift in the phase boundaries separating the different ordered states. For example, in a hexagonally packed cylindrical morphology in which the matrix surrounding the cylinders is composed of blocks with two different lengths, the variation in the distance separating the cylindrical interface from the edges of the hexagonal cell implies a dependence of the elastic energy of the matrix chains on their location within the unit cell. In order to minimize the variation in this energy, longer matrix chains might preferentially locate along lines extending

* To whom correspondence should be addressed.
† Current address: Department of Chemical Engineering and Materials Science, University of Minnesota, Minneapolis, MN 55455.
⊗ Abstract published in *Advance ACS Abstracts,* January 15, 1996.

0024-9297/96/2229-1204$12.00/0 

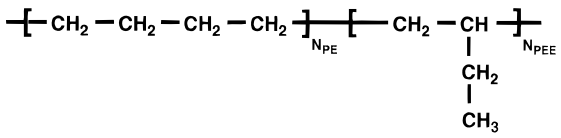


**Figure 1.** Molecular microstructure of PE−PEE diblock copolymer. The PE block contains about 6% PEE repeat units.

from the center to the vertices of the hexagonal unit cell, while the shorter chains might locate along the lines joining adjacent cylinders. Experiments in aqueous phospholipid systems[16] and block copolymers[17] have confirmed the importance of this variation in average chain conformation in stabilizing the cylindrical morphology; similar effects have been proposed in interpreting the phase behavior of $Ia\bar{3}d$/gyroid*-forming diblock copolymer−homopolymer blends.[7] Third, the phase boundaries are expected to become biphasic, spanning a finite range in segregation (i.e., temperature) for a system of constant composition, and the triple points of the monodisperse system will become constant-temperature three-phase lines (i.e., eutectic, eutectoid, peritectic, and peritectoid invariants[18,19]). Careful measurements will be required to assess the magnitude of these effects and thus determine the extent to which insights obtained in binary diblock blends may be extended to single-component systems.

The system chosen for the current study is poly(ethylene)−poly(ethylethylene) (PE−PEE); see Figure 1. This material has several characteristics that make it attractive for studies of block copolymer polymorphism. This is the least compatible pair of saturated hydrocarbon polymers we have investigated; that is, at a fixed temperature, it possesses the largest value of $\chi$, the Flory−Huggins interaction parameter, of all of the systems examined.[20] This leads to rather modest molecular weight requirements for ordering; a symmetric PE−PEE diblock ($f_{PE} = 0.5$) will order at or below 150 °C when the total number-average molecular weight ($M_n$) is greater than about 28 000. Due to the favorable combination of overall and entanglement molecular weights which lead to relatively short single-chain relaxation times at the temperatures of interest, this system is well suited for DMS measurements. The slight difference in electron density between PE and PEE facilitates SAXS analysis, while incorporation of deuterated monomer during the synthesis of the diblocks produces neutron contrast and permits analysis via SANS. Finally, since PE crystallizes when cooled below 108 °C, exposing this diblock to ruthenium tetraoxide at room temperature results in the preferential adsorption and reaction of the metal oxide vapors by the PEE block, thus producing mass thickness contrast and making the material suitable for examination via TEM.[21]

In this publication, we demonstrate that for pure diblocks with $f_{PE} < 0.5$, four ordered microstructures extend from moderate degrees of segregation to the order−disorder transition (ODT): spheres on a body-centered-cubic lattice (S), hexagonally packed cylinders (C), the bicontinuous $Ia\bar{3}d$/gyroid* phase (G), and lamellae (L); see Figure 2. The data suggest, but do not demonstrate, that a fifth morphology, hexagonally perforated layers (HPL), may separate the L and C mesophases at moderate or higher degrees of segregation. Similar results for blends of the $f_{PE} = 0.37$ and $f_{PE} = 0.46$ diblocks demonstrate the presence of four of these phases (C, G, HPL, and L) over a range in mean composition $\langle f_{PE} \rangle$ extending from 0.37 to 0.46.

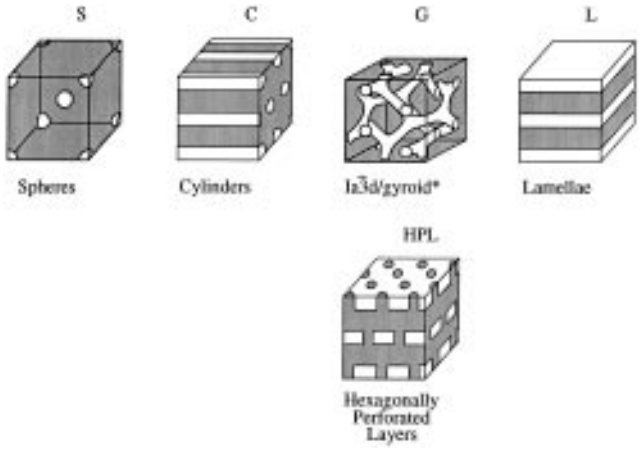


**Figure 2.** Schematic representations of the microstructures reported here in PE−PEE diblock copolymer melts. The minority component volume fraction ($f_{PE}$) increases from left to right across the diagram. The top four morphologies make contact with the disordered state while the HPL phase (tentatively identified in this publication) is bounded by the cylindrical, $Ia\bar{3}d$/gyroid*, and lamellar states.

## II. Experimental Procedures

**Synthesis.** The PE−PEE diblock polymers used in this study were prepared by a two-step process that has been described in previous publications;[20,22] a brief summary appears below. Precursor polydiene diblocks containing a predominantly 1,4-polybutadiene block (≈94%, *cis* and *trans* isomers) and an atactic 1,2-polybutadiene block (>99% 1,2 isomer) were anionically polymerized in cyclohexane using *sec*-butyllithium (Aldrich) as the initiator. The first block was prepared at 40 °C, followed by the addition at 20 °C of dipiperidinoethane (5:1 molar ratio relative to Li) and additional butadiene monomer. In one instance, perdeuterated butadiene (Cambridge Isotopes) was used in the second step in order to obtain neutron contrast (see below). Monomer, solvent, and the diamine additive were purified using established procedures; the initiator was titrated using the Gilman method. In all but one instance nearly complete conversion (>98%) was realized, allowing us to specify the block composition to within 0.01 in minority component weight fraction. The only exception was the reaction involving the perdeuterated butadiene in which a spurious termination reaction resulted in a yield of only 90%. Nevertheless, assuming that the first block ran to complete conversion (which is supported by the lack of 1,4-polybutadiene homopolymer), we are still able to assign a composition to this material.

Polydiene number-average molecular weights ($M_n$) were estimated based on the reaction stoichiometry. The reliability of these estimates was confirmed by the good agreement obtained between predicted and experimentally measured ODT temperatures in the final PE−PEE materials. Polydispersity indices were estimated by size exclusion chromatography based on polyisoprene calibration standards. The nondeuterated polydiene materials possessed indices between 1.05 and 1.07; the partially deuterated polymer has a somewhat higher value of 1.15.

The polydiene diblocks were saturated by hydrogenation (or deuteration) over a $Pd/CaCO_3$ heterogeneous catalyst in cyclohexane at 70 °C. The efficiency of this reaction was verified by solution $^1H$ NMR, conducted at elevated temperatures, to be greater than 99% conversion of all double bonds. Indirect confirmation was provided by a consistent PE melting temperature of 108 ± 2 °C for all samples; this value is consistent with an ethyl branch content of 1.5 per 100 backbone carbon atoms that results from 6% 1,2 addition in the 1,4-polybutadiene precursor. Crystallinity complicates SEC analysis of the hydrogenated material. Therefore, we have assumed that polydispersity is not affected by the hydrogenation procedure. Earlier studies with poly(ethylenepropylene)−poly(ethylethylene) (PEP−PEE) diblocks[22] support this assumption.

**Table 1. Molecular Characteristics of Pure Diblock Copolymers**

| specimen[a] | $f_{PE}$[b] | $M_n$[c] (kg/mol) | phases[d] |
|---|---|---|---|
| PE−PEE-8H | $0.50_0$ | 23.9 | L−136 °C−Dis |
| PE−PEE-3D | $0.49_0$ | 22.8 | L−120 °C−Dis |
| PE−PEE-18H | $0.45_6$ | 34.2 | L−276 °C−Dis |
| PE−PEE-14D | $0.43_0$ | 36.3 | (HPL)−154 °C−G−207 °C−Dis |
| PE−PEE-13D | $0.40_0$ | 41.5 | C−176 °C−G−250 °C−Dis |
| PE−PEE-16D | $0.37_4$ | 42.5 | C−294 °C−Dis |
| PE−PEE-11D | $0.25_2$ | 55.6 | C−238 °C−S−273 °C−Dis |

[a] H signifies hydrogenation of a polydiene precursor that contains a perdeuterous 1,2-polybutadiene block. D indicates deuteration of a fully hydrogenous precursor polymer. [b] $f_{PE}$ is the volume fraction of polyethylene. [c] Hydrogenous equivalent number-average molecular weight. The respective block molecular weights can be obtained using the ratio of densities, $\varrho_{PE}/\varrho_{PEE} = 0.983$. [d] L = lamellae; C = hexagonally packed cylinders; HPL = hexagonally perforated layers; S = bcc ($Im\bar{3}m$) packed spheres; G = $Ia\bar{3}d$/gyroid* cubic bicontinuous; Dis = disordered. Transition temperatures correspond to onset of variation in $G'(T)$ at fixed frequency during heating. Parentheses indicate a tentative phase assignment.

A list of the pure diblocks described in this work appears in Table 1. Number-average molecular weights were obtained by correcting the stoichiometric polydiene values for hydrogen addition. Polyethylene volume fraction, $f_{PE}$, was calculated from the independently measured amorphous densities of PE and PEE;[23] we ignore minor differences in melt thermal expansivity and assume $f_{PE}$ is independent of temperature.

**Blend Preparation.** Binary mixtures of the $f_{PE} = 0.37$ and $f_{PE} = 0.46$ diblock copolymers were prepared by codissolution in toluene at 90 °C followed by precipitation in methanol and drying in a vacuum oven at about 150 °C for ca. 12 h.

**Dynamic Mechanical Spectroscopy (DMS).** Viscoelastic measurements were performed on a Rheometrics RSAII solids analyzer with a shear sandwich fixture. Specimens were prepared by compression in vacuum between Teflon-covered plates at 140 °C to form films of uniform thickness. These films were then placed in the shear sandwich fixture for examination. Nitrogen was used as a purge gas to minimize oxidative damage to the materials. Two types of measurements were performed: isochronal experiments while slowly heating the sample (1 °C/min), and isothermal frequency scans. In both cases, the strain amplitude was between 2 and 5%.

**Transmission Electron Microscopy (TEM).** High-resolution TEM images were obtained from several of the PE−PEE specimens using a recently developed staining technique.[21] Most of the samples were shear-oriented to enhance the degree of long-range order in the initial morphology[1,2,24] and then annealed without shear at temperatures corresponding to specific ordered morphologies. After quenching in liquid nitrogen to crystallize the PE block and fix the ordered phase, sections of *ca.* 700 Å thickness were cut at low temperature (<−50 °C) with a Reichert ultramicrotome equipped with a diamond knife. Subsequent exposure of the section to ruthenium tetraoxide vapors resulted in the preferential absorption and reaction of the vapor in PEE-rich regions of the sample which generated sufficient mass thickness contrast to render the material suitable for TEM imaging.

**Small-Angle X-ray Scattering (SAXS).** Copper Kα X-rays were generated from a Rigaku RU-200BH rotating-anode X-ray machine equipped with a 0.2 × 2 mm microfocus cathode and Franks mirror optics. Samples were placed inside an evacuated sample chamber and maintained at a temperature of interest by a pair of thermoelectric devices (temperature range 0−185 °C, control accuracy ±0.05 °C). Two-dimensional diffraction images were collected with an image-intensified area detector designed around a Thomson CCD chip.[25] The sensitivity of the detector and the intensity of the beam line allowed collection of 2-D diffraction patterns with typical exposure times of 15 min. After collection, images were digitized, corrected for detector response characteristics, and then written to magnetic tape. Images were then integrated azimuthally along an arc ±15° from the axis normal to the polymer film surface to create one-dimensional traces of intensity vs scattering vector $q = 4\pi\lambda^{-1}\sin(\theta/2)$, where $\lambda$ and $\theta$ are the wavelength and scattering angle, respectively.

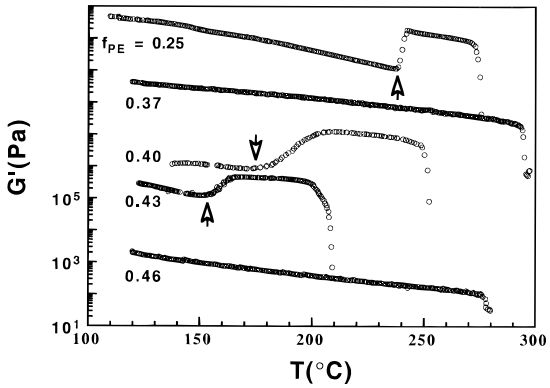


**Figure 3.** Isochronal ($\omega$ = 1 rad/s) dynamic elastic shear modulus measured at a heating rate of 1 °C/min for the five pure diblock copolymers listed in Table 1. These results were used to select materials likely to show order−order transitions (OOTs) and identify the range of temperatures where such transitions occur. The relatively rapid changes in $G'$ which characterize these transformations are indicated by arrows; the steep decline in $G'$ at the highest measurement temperatures signals the order−disorder transition (ODT).

**Small-Angle Neutron Scattering (SANS).** These experiments were conducted on the 12 m instrument located at the Risø National Laboratory in Roskilde, Denmark, using neutrons with a wavelength of 6.0 Å and a wavelength spread ($\Delta\lambda/\lambda$) of 0.09 and an area detector. The 2-D scattering intensity data were corrected for spatial variations in the detector sensitivity. Binary blends of the deuterium-labeled diblock ($f_{PE}$ = 0.46) and an unlabeled material ($f_{PE}$ = 0.37) were prepared as described above and oriented in a previously described *in-situ* reciprocating shear device.[1,2,24] Specimens were held in temperature-controlled (±1 °C) aluminum shear cells[26] with fixed gaps of 0.6, 0.9, or 1.2 mm. Steady reciprocating shear was applied to macroscopically align certain melt microstructures. After initial alignment, subsequent annealing was performed in the absence of shear to develop the long-range order of the initial microstructure and to drive the sample through phase transitions. The use of a well-aligned initial state exposes aspects of the lattice symmetry that are associated with the angular correlation of the principal Bragg reflections. This facilitates identification of diffracting microstructures and the recognition of epitaxial relations between the different morphologies.

## III. Results

**A. Single-Component Materials.** Prior work has demonstrated that the experimental methods used in this study are effective in establishing block copolymer phase behavior.[1−3,6,7,17,20,24,27] We have, therefore, refrained from providing detailed descriptions of the results obtained for each sample, choosing instead to concentrate on those materials that exhibited behavior of particular interest.

Perhaps the most efficient method of estimating order−order and order−disorder transition temperatures ($T_{OOT}$, $T_{ODT}$) in a previously unexamined material is to slowly heat the specimen while monitoring its viscoelastic properties. At sufficiently low frequencies, the physical properties are dominated by the microdomain structure, and changes in this structure are directly reflected in both the elastic ($G'$) and loss ($G''$) components of the complex dynamic shear modulus. Examples of this behavior appear in Figure 3. Five single-component specimens were heated at 1 °C/min while $G'$ was measured at a frequency of 1 rad/s. In two of these materials ($f_{PE}$ = 0.37 and 0.46), $G'$ decreases with increasing temperature until a precipitous drop is observed at the ODT. In the remaining specimens ($f_{PE}$

= 0.25, 0.40, and 0.43), a sharp increase in $G'$ precedes the ODT, suggestive of a phase transition between ordered morphologies.

A more robust comparison of the rheological properties associated with the different ordered morphologies is obtained through isothermal frequency scans. Five spectra, corresponding to the five microstructures observed in neat PE−PEE diblocks, appear in Figure 4; the microstructural assignments shown in the figure have been determined through a combination of SANS, SAXS, and TEM as will be described in subsequent paragraphs. As the dimensionality of the microstructure increases, the overall elasticity of the system as measured by $G'$ increases. Quite remarkably, the two cubic phases (spheres and $Ia\bar{3}d$/gyroid*) exhibit nearly identical viscoelastic properties. In both cases, there is a crossover at the lowest measurement frequencies to a more dissipative but nonterminal response. Regardless of the dynamical processes reponsible for the complex rheological properties shown in Figure 4, measurement of $G'(\omega)$ and $G''(\omega)$ provides a useful "fingerprint" that aids in the identification of each microstructure.

By themselves, rheological measurements serve only to indicate that a transition may have occurred; investigation with a more direct technique is necessary to identify the morphologies on either side of a (possible) order−order transition. After determining regions of interest with rheological techniques, subsequent investigation via SAXS, SANS, and/or TEM was used to establish the microstructure of the material. Figure 5 presents representative micrographs obtained from the pure diblocks. All of these materials (except for $f_{PE}$ = 0.25, which was merely annealed) were shear-oriented above the melting temperature of the PE block in order to facilitate identification of the ordered morphology. The images shown present views coincident with the shear direction. As this is the axial direction assumed by hexagonally packed cylinders when subjected to a shear field,[26,28] this is the most useful projection for discriminating between cylindrical and layered morphologies. Hexagonally packed cylinders are indicated for specimens in which $f_{PE}$ = 0.25 and 0.40; a lamellar structure is evident for $f_{PE}$ = 0.46. The low-temperature morphology of the $f_{PE}$ = 0.43 specimen (108 < $T \leq$ 154 °C) is certainly not cylinders since a hexagonal pattern was not found in any of the many images obtained from this material. A layered microstructure can be discerned, but it lacks the long-range order present in the lamellar image that characterizes the $f_{PE}$ = 0.46 sample. Although this projection is consistent with the HPL morphology, the TEM image lacks definitive evidence of regularly spaced perforations as is found in PI−PS,[3−5] PE−PEP,[2] and PS−PVP[27] specimens. This might be a consequence of the thickness of the sections (*ca.* 700 Å) or of damage incurred during the process of rapid crystallization while preparing the material for TEM analysis;[21] presumably, this damage does not prevent identification of the sample morphology in the other PE−PEE materials studied. Unfortunately, satisfactory images of the high-temperature phase of the $f_{PE}$ = 0.40 (176 ≤ $T \leq$ 250 °C) and 0.43 (154 ≤ $T \leq$ 207 °C) specimens proved difficult to obtain; we postulate that rapid crystallization of the PE block may disrupt these microstructures. However, a satisfactory picture of the spherical morphology was obtained from the high-temperature phase of the $f_{PE}$ = 0.25 material (238 ≤ $T$ ≤ 273 °C) as shown in Figure 5.

SAXS examination of unsheared (macroscopically isotropic) specimens of the $f_{PE}$ = 0.40 and 0.43 samples

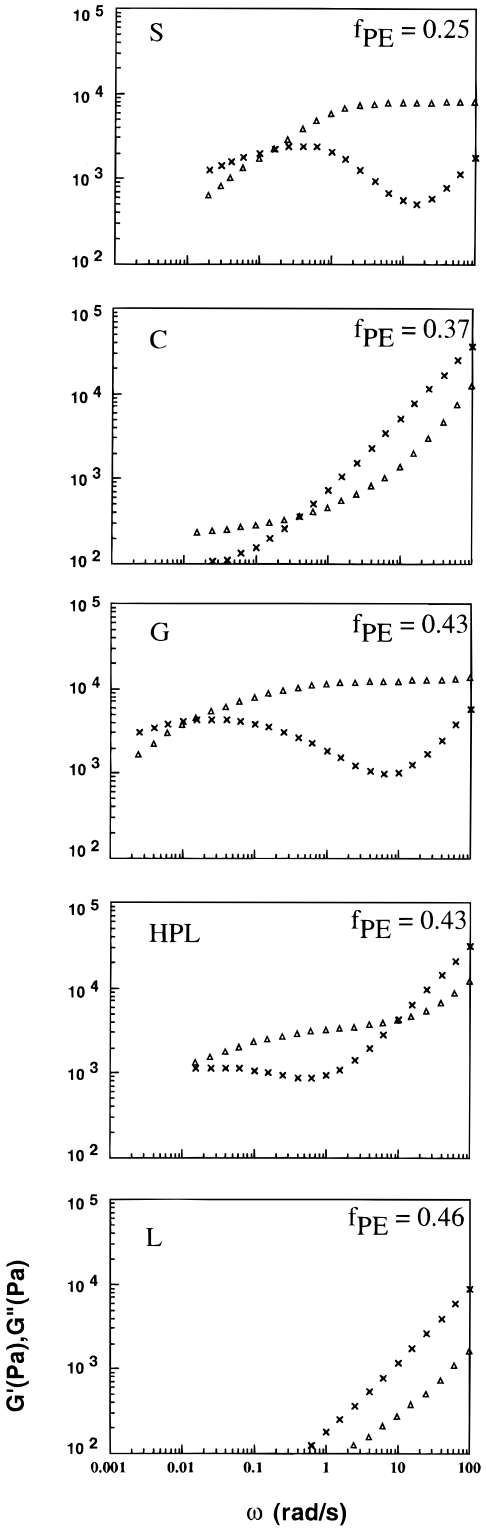


**Figure 4.** Selected isothermal frequency scans from pure diblock copolymers listed in Table 1 that illustrate the qualitative differences in dynamic mechanical response between the five microstructures discussed in this paper: (Δ) − $G'$; (×) − $G''$. The microstructural assignments associated with each plot have been made through a combination of SAXS and TEM as described in the text. Of particular interest is the similarity between the spectra for the *G* (cubic bicontinuous) and *S* (spherical) microstructures. From top to bottom the measurement temperatures (°C) were 245, 120, 180, 120, and 146.

produced diffraction consistent with the low-temperature phase assignments made by TEM, suggesting that the sample morphology is unaffected by application of the shear field used in conducting the rheological measurements and preparing the materials for micros-

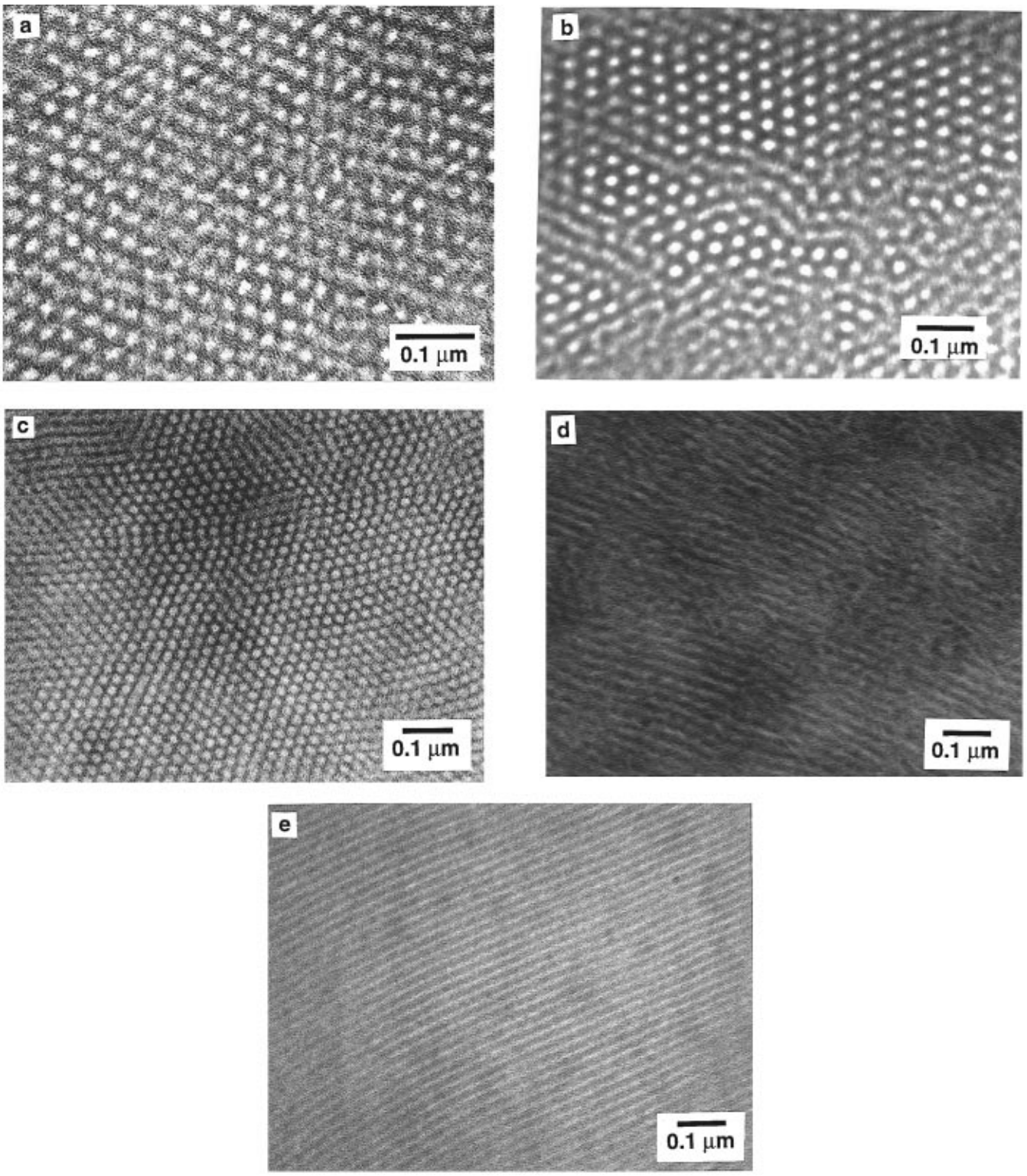


**Figure 5.** Transmission electron micrographs obtained from pure PE−PEE diblock copolymers after quenching in liquid nitrogen followed by cryoultramicrotoming and staining with ruthenium tetraoxide. Light and dark regions correspond to PE and PEE microdomains, respectively. In the $f_{PE} = 0.40$, 0.43, and 0.46 materials, the specimen was shear-aligned prior to examination to facilitate imaging; the incident electron beam is parallel to the shear direction. (a) $f_{PE} = 0.25$ high-temperature phase (spheres); (b) $f_{PE} = 0.25$ low-temperature phase (cylinders); (c) $f_{PE} = 0.40$ low-temperature phase (cylinders); (d) $f_{PE} = 0.43$ low-temperature phase (tentatively HPL); (e) $f_{PE} = 0.46$ (lamellae).

copy. Representative scattering patterns taken after several hours of annealing at temperatures above and below the rheologically determined OOT temperatures appear in Figure 6. Both samples produce well-defined principal reflections at 120 °C. Unfortunately, the low-temperature phase microstructure of the $f_{PE} = 0.43$ material cannot be identified due to the absence of higher order reflections. A weak higher order peak is discernible in the trace from the $f_{PE} = 0.40$ sample. Although diffraction reflections at position ratios of 1:2 are characteristic of a lamellar morphology, such scattering is also consistent with the hexagonally packed cylindrical structure observed via TEM, as the location of the minimum in the structure factor for cylinders of this minority component volume fraction will result in an extremely low intensity for the $\sqrt{3}$ peak. Subsequent annealing of both materials at 175 °C induces a transformation to a morphology that exhibits diffraction

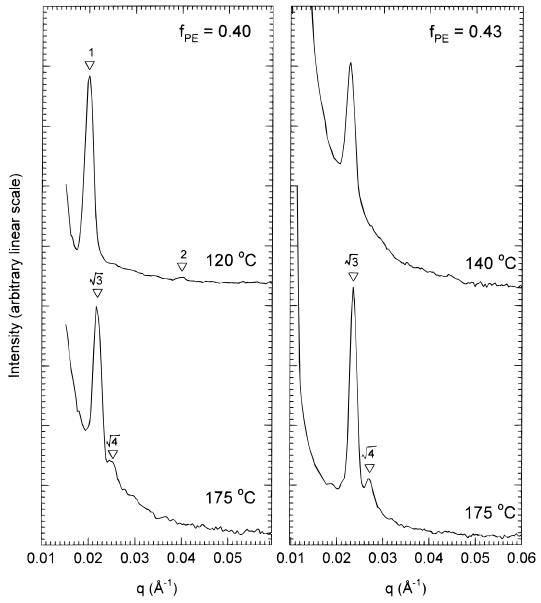


**Figure 6.** One-dimensional SAXS profiles recorded from the low- and high-temperature phases of unoriented $f_{PE} = 0.40$ and 0.43 diblocks. Both the relative spacings ($\sqrt{3}$:$\sqrt{4}$) and intensities (10:1) of the reflections seen in the two high-temperature profiles are consistent with the $Ia\bar{3}d$/gyroid* morphology.

reflections at position ratios of $\sqrt{3}$:$\sqrt{4}$ in which the intensity of the higher order peak is approximately 10% of that of the principal reflection, which is consistent with the $Ia\bar{3}d$/gyroid* microstructure.[3,7] Annealing behavior similar to that observed in the $f_{PE} = 0.43$ material, in which a layered morphology characterized by a single diffraction reflection at low temperatures gradually transforms to the $Ia\bar{3}d$/gyroid* structure upon prolonged exposure to elevated temperatures, has been previously observed between 120 and 140 °C in $f_{PI} = 0.66$ PI−PS diblocks.[7] Thermotropic transitions between C and G have been identified in $f_{PI} = 0.73$ PI−PS starblocks[10] and several PI−PS,[3,28] PS−PVP,[6,27] and PEP−PEE[14,30] diblocks. These results indicate that the G phase can transform to cylinders, or vice versa, with heating. However, a pronounced hysteresis has been reported when cooling the bicontinuous phase below an order−order transition.[3,27,29]

Confirmation of the equilibrium nature of the observed microstructures was obtained for the $f_{PE} = 0.37$ and 0.46 materials (which do not exhibit thermotropic order−order transitions) by examination of samples which were first heated above $T_{ODT}$ and then quenched to a lower temperature and annealed. TEM analysis indicated cylinders and lamellae, respectively. A similar approach was used to analyze the $f_{PE} = 0.40$ sample. In this case, the material was heated on the rheometer until the disordered state was formed and then rapidly quenched (without shear) to 115 °C, i.e., well below $T_{ODT}$ and $T_{OOT}$ for this specimen, but above the melting temperature of the PE block. Within approximately 60 s, the sample was cooled to within several degrees of the target temperature. Then, the temperature was raised to a value near $T_{OOT}$ (determined from the rheological data in Figure 3), and the development of order was monitored through isothermal frequency scans. Figure 7 depicts the evolution of $G'$ ($\omega = 0.1$ rad/s) at temperatures of 158, 162, 168, 173, and 178 °C. The significant difference in moduli obtained after prolonged annealing at 162 and 168 °C suggests that the phase boundary separating the cylindrical and $Ia\bar{3}d$/gyroid* morphologies lies between these two tempera-

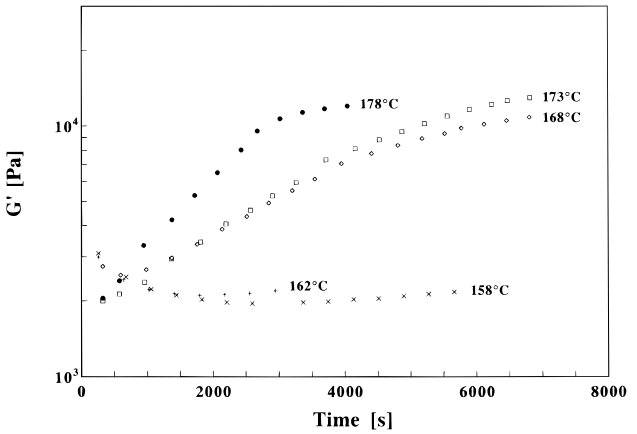


**Figure 7.** Development of $G'(\omega = 0.1$ rad/s) in the $f_{PE} = 0.40$ pure diblock specimen after rapidly cooling to 115 °C from the disordered state (260 °C) followed by immediate heating to the indicated temperature. This quenching process required less than 300 s. SAXS measurements indicate that at high temperatures, a bicontinuous morphology grows, while at low temperatures, a cylindrical morphology develops. The differences in rheological response observed at 162 and 168 °C suggest that the C-to-G transition temperature lies between these temperatures.

tures; the full frequency scans resemble those associated with each microstructure in Figure 4. This transition temperature is 8−14 deg lower than that obtained from Figure 3 (see Table 1). We attribute this disparity to finite nucleation and growth rates coupled to the heating rate employed; the true equilibrium phase transition temperature probably lies between 162 and 168 °C.

The equilibrium nature of the microstructures observed in the $f_{PE} = 0.25$ and 0.43 materials was confirmed by demonstrating the thermoreversible nature of the transitions. Such measurements are frequently complicated by the considered hysteresis often associated with thermotropic order−order transitions in block copolymers.[1−3,7,17,24] After annealing at elevated temperatures to form the $Ia\bar{3}d$/gyroid* morphology, cooling the $f_{PE} = 0.43$ specimen to temperatures at which the (presumed) HPL morphology is observed upon heating resulted in the eventual return of the initial microstructure,[3] as evidenced by the frequency independence of $G'$ and $G''$. The pronounced hysteresis observed upon quiescently supercooling the sample complicates identification of the (presumed HPL)−$Ia\bar{3}d$/gyroid* transition kinetics; although dynamic shearing can reduce this difference in transition temperatures to some degree, it is unclear that results obtained with the latter technique can be extended to the field-free case. Similar (though less problematic) hysteresis was observed in the C-to-S transition exhibited by the $f_{PE} = 0.25$ polymer, similar to what we reported for the $f_{PEP} = 0.25$ PEP−PEE material.[24]

Figure 8a summarizes our measurements of phase behavior in the single-component (pure diblock) PE−PEE specimens. Ordered phase symmetries could be assigned to all phases in the pure materials with the exception of the low-temperature state of the $f_{PE} = 0.43$ diblock. TEM and rheological data for this specimen suggest a layered microstructure that we tentatively associate with the HPL phase. As these data include DMS, TEM, and SAXS measurements, accurate determination of a phase diagram for the pure diblock materials requires knowledge of the degree to which phase boundaries identified through rheological means match those obtained in the absence of a shear field. Certainly, shear is expected to influence phase behavior

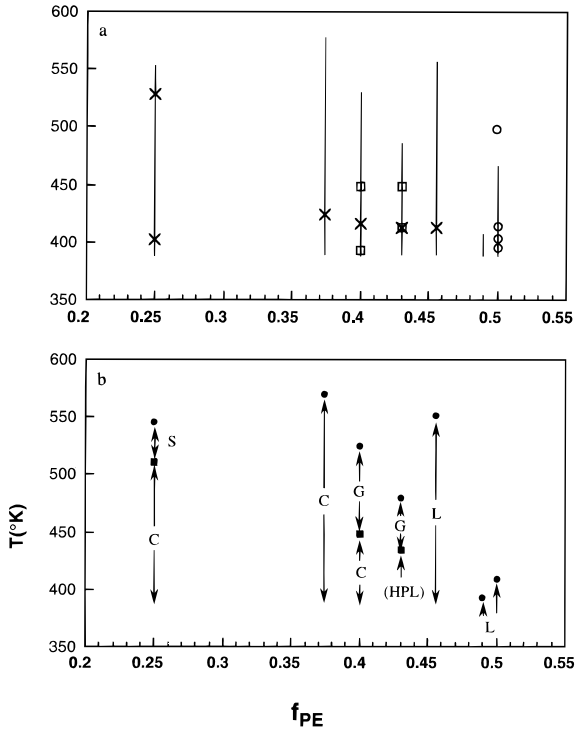


**Figure 8.** (a) Summary of experiments performed with the pure diblock copolymers as a function of temperature and the minority block volume fraction. Vertical lines identify the temperature range for dynamic mechanical spectroscopy (DMS) measurements; □ symbols indicate SAXS on unsheared specimens; ○ symbols denote SANS on sheared and unsheared specimens; × symbols identify annealing temperature prior to liquid nitrogen quenching for TEM analysis. (b) A "phase diagram" for PE−PEE diblock copolymers, constructed based on the DMS, SAXS, SANS, and TEM results. ● and ■ symbols mark OOT and ODT temperatures, respectively, determined from isochronal $G'(T)$ measurements (see Figure 3). The S, C, G, and L morphologies have been clearly identified while the HPL state is a tentative assignment.

to some degree; in separate work we have demonstrated the effect of large-amplitude ($|\gamma| \leq 100\%$) fields on the location of the ODT in weakly segregated PEP−PEE melts.[31,32]

These effects can be assessed by examining the shear rates and amplitudes necessary to produce changes in $T_{OOT}$ and $T_{ODT}$. Earlier experiments with symmetric PEP−PEE diblock copolymers[33] have shown that the lamellar-to-disorder transition temperature is unaffected by variations in the applied frequency and shear strain amplitude when $|\gamma| \leq 20\%$. We have also found general consistency between SANS- and DMS-determined ODT temperatures (within 2 °C) from a host of asymmetric diblock materials that contain spherical, cylindrical, and bicontinuous ordered phases, leading us to conclude that the modest deformations imposed during presently reported rheological measurements did not measurably alter $T_{ODT}$. However, the magnitude of $G'$ and $G''$ when in an ordered state does depend on strain amplitude above a certain value. The onset of such nonlinearity can be attributed to domain orientation and/or local microstructural rearrangement. Winey et al.[34] have reported a nonlinear viscoelastic response in lamellar PS−PI diblock melts for strain amplitudes above roughly 1%. In layered and cylindrical microstructured materials, the associated strain softening is usually nonrecoverable since it derives from the macroscopic alignment of domains. Cubic microstructures also strain-soften[24] but for a different reason: shearing induces defects (perhaps even disordering) in the solid state. These defects can be removed by annealing upon

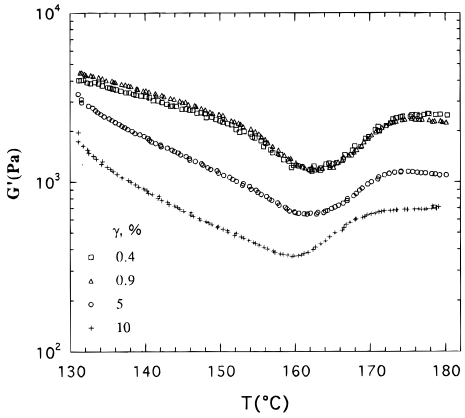


**Figure 9.** Strain amplitude ($|\gamma|$) dependence of $G'(\omega=0$ rad/s) while heating the $f_{PE} = 0.43$ pure diblock at 1 °C/min. Prior to making each temperature scan, the specimen was heated above $T_{ODT}$ and then rapidly cooled to 130 °C. The upturn in $G'$ between 160 and 164 °C, which we associate with an order−order transition, is only weakly dependent on $\gamma$ between 1 and 10%. For $|\gamma| < 1\%$, a linear response is observed.

cessation of the deformation, leading to recovery of the original viscoelastic properties.

The order−order phase transitions in the PE−PEE materials could be influenced by both these effects, which could compromise the reliability of the DMS determination of $T_{OOT}$. Therefore, we examined the sensitivity of $G'(T)$ to variations in strain amplitude in several pure and blended samples between $|\gamma| = 0.4\%$ and 10%; representative results for the $f_{PE} = 0.43$ sample are shown in Figure 9. These measurements were made at 0.5 rad/s while heating the specimen at 1 °C/min; the thermal treatment prior to each heating sequence consisted of disordering the material ($T > T_{ODT}$) followed by rapid cooling to 130 °C. For strain amplitudes below approximately 1%, $G'(T)$ is essentially independent of $|\gamma|$. We associate $T_{OOT}$ with the strong upturn in elasticity that occurs at about 162 °C. As $|\gamma|$ is increased to 5% and 10%, the entire $G'(T)$ curve shifts down, indicating that the material strain-softens. However, the location of the feature identified with $T_{OOT}$ is reduced by only 3 °C when the largest strain amplitude is applied to the material. (All these transition temperatures are slightly higher than the ones reported in Table 1, which we attribute to a different thermal history.) Separate experiments conducted with the high-temperature phase at 190 °C show that for $|\gamma| < 1\%$ the viscoelastic response is independent of $|\gamma|$ (i.e., linear) over the entire accessible frequency range ($10^{-3} < \omega < 10^2$ rad/s). These results, when combined with small-angle scattering evaluation of unsheared materials, demonstrate that dynamic shearing during the DMS measurements reported here did not significantly affect the (quiescent) phase state, or phase transition temperatures, and conform that rheological measurements are a valid tool for determining $T_{OOT}$ when conducted at, or near, linear viscoelastic conditions. (Of course, we cannot exclude the possibility that the symmetry-breaking effects of a shear field may induce slight differences in phase behavior, even at the smallest strain amplitudes.)

A "phase diagram", constructed from the data summarized in Figure 8a, appears in Figure 8b. As $f_{PE}$ is not a true intensive variable, this is not a proper thermodynamic representation, but it is the most convenient way to convey our results. Order−order and order−disorder phase transition temperatures have been taken from the isochronal $G'(T)$ data found in Figure 3; the onset of change in $G'$ is used as the

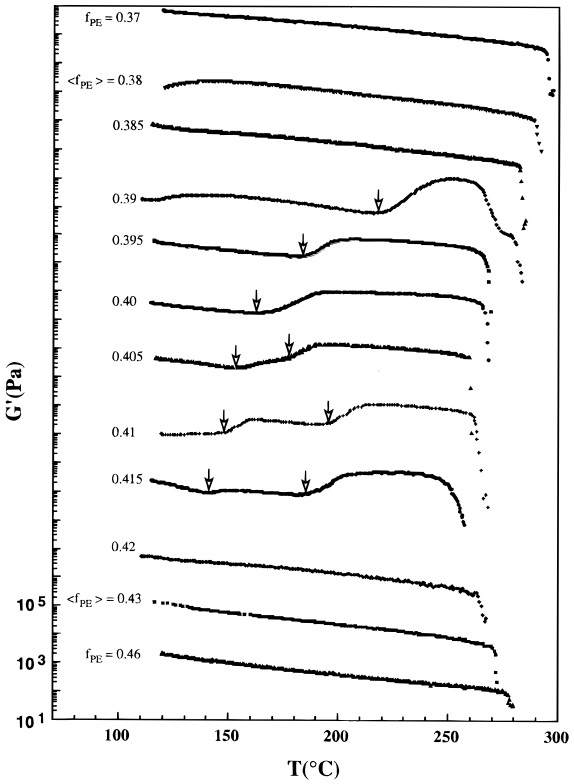


**Figure 10.** Isochronal ($\omega$ = 0.5 rad/s) dynamic elastic shear modulus measured at a heating rate of 1 °C/min for blends of the $f_{PE}$ = 0.37 and 0.46 PE−PEE diblock copolymers. $\langle f_{PE} \rangle$ refers to the overall PE volume fraction. As in Figure 3, potential OOT temperatures are indicated by the arrows. The steep decline in $G'$ at the highest temperatures indicates the ODT. Data sets above $f_{PE}$ = 0.46 have been shifted up progressively by a factor of 100.

criterion for assignment of a phase transition temperature. In principle, equilibrium phase transition temperatures should be assigned based on a common point determined by heating and cooling experiments. The large hysteresis effect associated with block copolymer order−order transitions makes this procedure impractical. Therefore, we have used heating experiments to identify $T_{OOT}$. Because these have been obtained at a finite heating rate, they likely overestimate the equilibrium values. An estimate of this inaccuracy was given for the $f_{PE}$ = 0.40 material (8−14 °C) in the preceding paragraphs.

**B. Two-Component Materials (Blends).** As described in the Introduction, experimentally measuring the phase behavior for pure block copolymers with a high degree of resolution in $f$ would require an exhaustive synthetic effort. In order to explore the region of bicontinuous phase stability identified in the pure diblocks ($0.37 < f_{PE} < 0.46$; see Figure 3), blends of the $f_{PE}$ = 0.37 and 0.46 polymers were prepared and characterized via DMS, SANS, and TEM. The overall minority component volume fraction of each blend is denoted by $\langle f_{PE} \rangle$.

A compendium of isochronal $G'(T)$ scans for these blends is presented in Figure 10. Samples with blend volume fractions of less than 0.385 or greater than 0.420 display monotonically decreasing curves of $G'$ vs temperature, suggesting the presence of a single ordered morphology at temperatures less than $T_{ODT}$. In blends with $\langle f_{PE} \rangle$ = 0.390, 0.395, and 0.400, a single thermally induced order−order transition is observed, as evidenced by a discontinuous jump in the slope of $G'(T)$ similar to that seen in the single-component materials

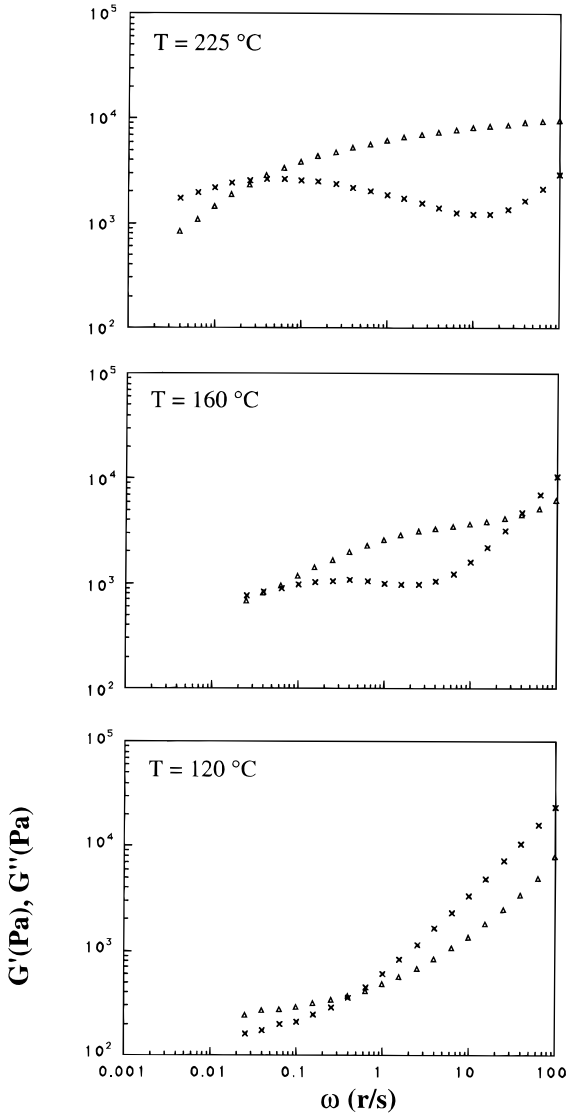


**Figure 11.** Selected isothermal frequency scans from the $\langle f_{PE} \rangle$ = 0.410 blend. SANS indicates that this material adopts the $Ia\bar{3}d$/gyroid* morphology at 225 °C as described in the text. Compare with the rheological "fingerprints" shown in Figure 4.

(compare with Figure 3). For $f_{PE}$ = 0.405, 0.410, or 0.415, two such transitions are seen. The isothermal frequency dependence of $G'(\omega)$ and $G''(\omega)$ in all of the observed blend phases generally mimics those documented in the single-component materials; compare the results shown in Figure 4 with the three representative spectra, taken from the $\langle f_{PE} \rangle$ = 0.410 blend, that appear in Figure 11. The rheological data suggest, but do not prove, that the low-, intermediate-, and high-temperature microstructures of this blend are cylinders, hexagonally perforated layers, and an undetermined morphology with three-dimensional symmetry (either gyroid*/$Ia\bar{3}d$ or a body-centered-cubic lattice of spheres).

The microstructures of these diblock blends were identified via SANS using a protocol similar to that employed in a number of earlier publications: after alignment of the initial morphology through the application of a shear field at a particular annealing temperature, the shear field was removed and samples were heated or cooled to a temperature of interest in order to follow morphological transitions in the absence of deformation. Representative contour plots from the $\langle f_{PE} \rangle$ = 0.410 blend are shown in Figure 12. The patterns at 115 and 160 °C were recorded after shearing

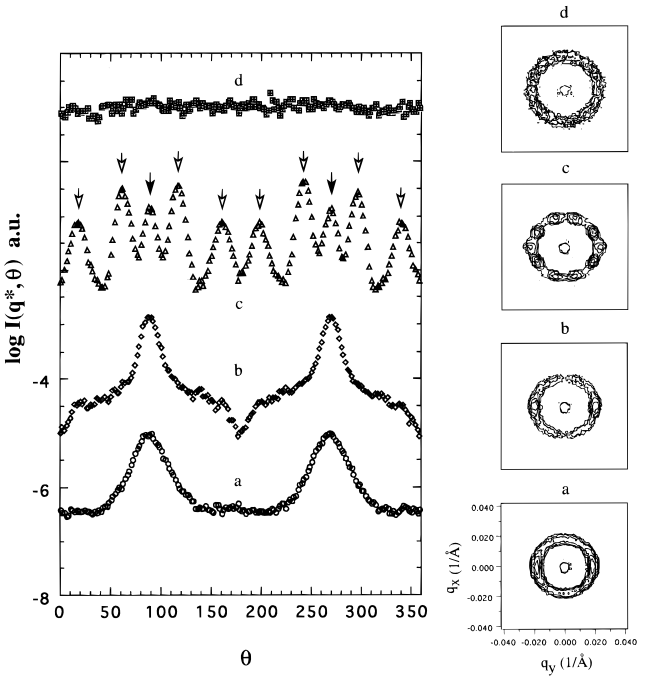


**Figure 12.** SANS images recorded from the $\langle f_{PE} \rangle = 0.410$ blend after orientation with the *in-situ* shearing device. The azimuthal dependence of the peak scattered intensity appears to the left where $\theta = 0$ corresponds to the positive $q_x$ direction. Successive curves have been shifted vertically by 2.5 orders of magnitude. Open and filled arrows identify {211} and {220} reflections, respectively. (a) $T = 115$ °C, data taken after shearing; (b) $T = 160$ °C, data taken after shearing; (c) $T = 210$ °C, heated from (b) without shear; (d) $T = 269$ °C, heated from (c) without shear.

followed by annealing at these temperatures, while the images captured at 210 and 269 °C were obtained after quiescent annealing of the material prepared at 160 °C at the indicated temperature. The azimuthal distribution of the total scattered intensity within the range from $0.7q^*$ to $1.3q^*$, where $q^*$ is the location in reciprocal space of the principal reflections, is also shown.

In the low-temperature state (115 °C), shearing orients the sample microstructure, although the two principal reflections are not well defined azimuthally. Due to the absence of higher order reflections, we cannot identify the microstructure from this result. However, TEM images, obtained after annealing a shear-aligned specimen for 6 days at 134 °C, indicate a lamellar morphology as illustrated in Figure 13. Azimuthally sharper reflections superimposed on abnormally broad bases of undetermined origin appear in the diffraction from the intermediate state (160 °C). Again, the absence of higher order reflections precludes the identification of the diffracting morphology; this state did not produce interpretable TEM images for shear-oriented and annealed specimens.

Heating the shear-oriented blend to higher temperatures produces darmatic changes in the SANS profile; see Figures 12 and 14. Ten well-defined reflections appear at azimuthal angles ($\phi$) of ±20°, ±62°, ±90°, ±118°, and ±160° with respect to the shear direction ($\phi = 0$). Careful analysis of the data in Figure 14 reveals two length scales: $q = 0.0207$ Å$^{-1}$ reflections at $\phi = \pm 20, \pm 62°, \pm 118°$, and ±160°; and $q = 0.0237$ Å$^{-1}$ reflections at $\phi = \pm 90°$. Due to the intrinsically poor $q$ resolution of the SANS instrument, this difference can only be established when these reflections are separated azimuthally. (We selected a rather broad band of $q$ values when calculating $I(q^*,\theta)$ in Figure 11 in order to optimize the angular resolution.) To within

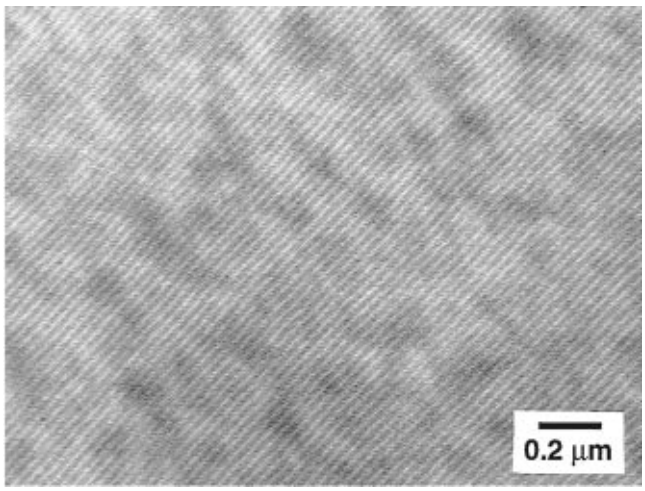


**Figure 13.** Transmission electron micrographs obtained from the $\langle f_{PE} \rangle = 0.41$ blend after shear alignment and annealing at 134 °C for 6 days. A lamellar morphology is indicated by this image.

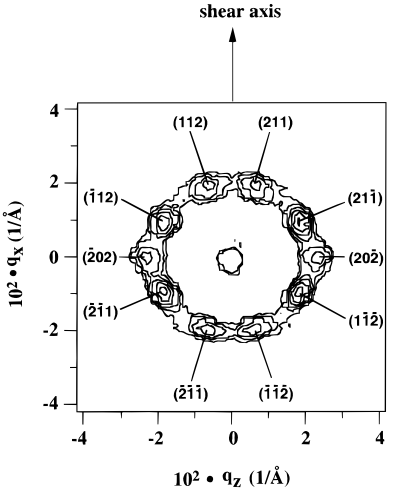


**Figure 14.** Expanded view of the SANS image shown in Figure 12 for the $\langle f_{PE} \rangle = 0.410$ blend at 210 °C. Reflections are indexed with the [111] direction coincident with the shearing direction. As described in the text, the presence of this complement of {211} and {220} reflections indicates epitaxial growth of the $Ia\bar{3}d$/gyroid* structure with some degree of mosaicity from a layered microstructure with a "parallel" orientation.

experimental error (approximately 1% of the absolute value of $q$), these reflections appear at position ratios of $\sqrt{3}:\sqrt{4}$ and are therefore consistent with the $Ia\bar{3}d$/gyroid* morphology. The azimuthal spacings of the peaks are characteristic of {211} and {220} reflections, providing further evidence for this phase assignment.

The azimuthal dependence of these ten reflections indicates that the [111] axis of the cubic phase is coincident with the shear direction, in agreement with previous results on epitaxial growth of the $Ia\bar{3}d$/gyroid* microstructure from oriented grains of cylinders[6,27] and hexagonally perforated layers.[3] The occurrence of this complement of {211} and {220} reflections requires a certain amount of variation in the microstructure director, or "mosaicity". However, the presence of {220} reflections at $\phi = \pm 90°$, combined with essential complete absence of {211} reflections at these angles, establishes the principal orientation of the unit cell as described above and sketched in Figure 15. Perfect alignment of the $(1\bar{2}1)$ plane parallel to the shear plane, with [111] parallel to the shear axis, would produce only $(20\bar{2})$ and (202) reflections at $\phi = \pm 90°$ when the neutron

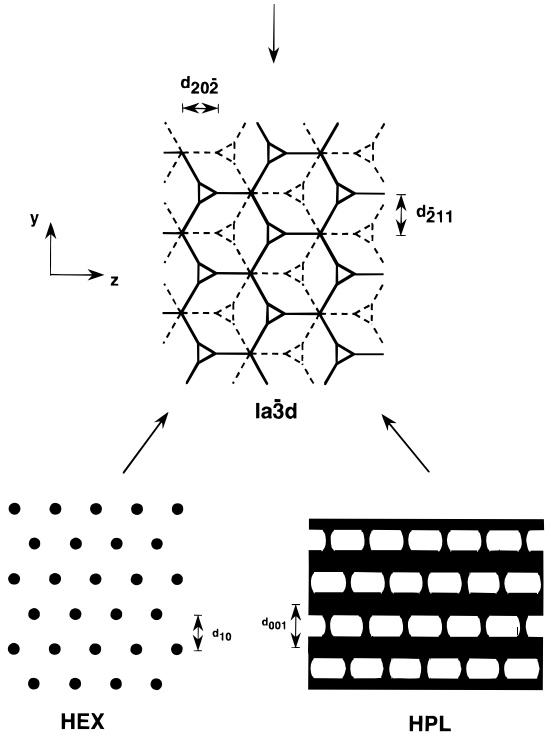


**Figure 15.** Epitaxial relationships for growth of the $Ia\bar{3}d$/gyroid* phase from hexagonally packed cylinders and hexagonally perforated layers. These images are projected along the shear direction, which is coincident with the [111] axis of the cubic phase. The arrow above the $Ia\bar{3}d$/gyroid* structure indicates the direction of the neutron beam for the SANS result shown in Figure 14.

beam is directed normal to $(1\bar{2}1)$. However, a mere 9.6° relative to this direction accounts for the eight {211} reflections identified in Figure 12. (Note that a 30° rotation about the [111] axis is needed to place the $(\bar{2}11)$ and $(2\bar{1}\bar{1})$ reflections at ±90°, which accounts for their absence in Figure 14.) Such microstructural distortion might result from deformation during the morphological transformation or from some degree of imperfection in the orientation of the low-temperature phase.

This assessment also provides an indirect clue as to the nature of the intermediate-temperature phase from which the bicontinuous structure grew. Lamellar, hexagonally perforated layer, and cylindrical microstructures have been shown to orient in two distinct ways when subjected to shear. These are referred to as the "parallel" and "perpendicular" orientations. In a layered structure (lamellar or HPL), the "parallel" form places the layers in the shear plane, i.e., the layer normals are parallel to the shear gradient, while in the "perpendicular" orientation, the layer normal is perpendicular to both the shear direction and the shear gradient.[35] In hexagonally packed cylinders, the "parallel" orientation places the cylinder director parallel to the shear direction, while the "perpendicular" orientation places the director along the shear gradient.[26] In previous work, we have established epitaxial relationships between the $Ia\bar{3}d$/gyroid* morphology and the cylindrical and layered morphologies: Layered (001) ↔ $Ia\bar{3}d$ (211) and cylinder (10) ↔ $Ia\bar{3}d$ (211). Similar relationships have been ordered in lyotropic liquid crystals.[36,37] Based on these relationships, the scattering patterns shown in Figures 12 and 14 suggest that the $Ia\bar{3}d$/gyroid* morphology grew from a "parallel" orientation of the intermediate structure. In a separate study,[38] we have found that azimuthally resolved reflections such as those seen in Figure 13 *do not* occur when

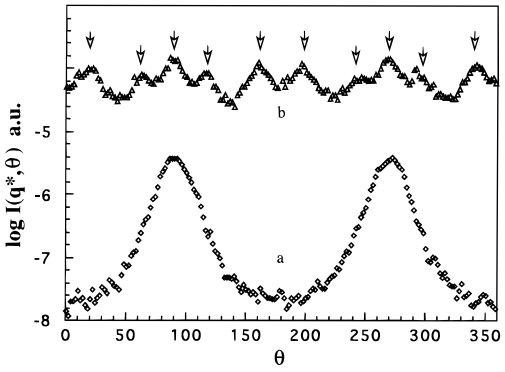


**Figure 16.** Azimuthal plots of peak SANS intensities from the $\langle f_{PE} \rangle = 0.400$ blend specimen. The arrows identify the predicted location of {211} cubic reflections assuming that the [111] direction is oriented coincident with the shear direction. (a) $T = 150$ °C, data taken after shearing; (b) $T = 190$ °C, heated from (a) without shear.

the $Ia\bar{3}d$/gyroid* phase evolves from "parallel" lamellae. Not surprisingly, in-plane order seems to be required to guide three-dimensional epitaxy from a layered morphology. Therefore, we rule out lamellae as a possible structure for the intermediate state, a conclusion that is also suggested by the qualitative differences in the isothermal rheological properties of the intermediate and lamellar morphologies (compare Figures 4 and 11).

SANS examination of the $\langle f_{PE} \rangle = 0.400$ blend, which exhibited only one thermotropic transition in isochronal rheological measurements (see Figure 10), appears in Figure 16. Data taken after shear-orienting the material at 150 °C exhibits two (azimuthally and radially) sharp reflections characteristic of an oriented low-symmetry microstructure. Upon heating to 190 °C in the absence of shear, a ten-spot pattern develops, with the azimuthal locations of the reflections consistent with a {211} assignment, and hence suggesting the presence of the $Ia\bar{3}d$/gyroid* phase. (The absence of higher order reflections and the lack of TEM data make this a tentative conclusion.) However, the spots are not as well resolved as in the $\langle f_{PE} \rangle = 0.410$ blend. Furthermore, all of the reflections appear at a single value of $q$; and while the $\phi = 62°$ and 118° reflections are brightest in the $\langle f_{PE} \rangle = 0.410$ blend, these were the weakest reflections for the $\langle f_{PE} \rangle = 0.400$ material. A similar result was obtained in an earlier study involving epitaxial growth of the $Ia\bar{3}d$/gyroid* microstructure from a shear-oriented cylindrical state.[6] Those observations suggest that the $Ia\bar{3}d$/gyroid* microstructure grew at high temperature from a hexagonal cylinder low-temperature state. Additional experiments with rapidly quenched shear-aligned specimens that were cut after alignment and examined with the neutron beam along the shear axis revealed diffraction characteristic of hexagonal symmetry, supporting this low-temperature phase assignment.

Figure 17a summarizes the blend experiments as a function of measurement temperature and $\langle f_{PE} \rangle$; a "phase diagram" constructed from these data appears as Figure 17b.

## IV. Discussion

The phase behavior illustrated in Figures 8 and 17 is remarkably similar to that which has recently been reported for PI−PS diblock copolymers[3] with $f_{PI} < 0.5$. In that study, the bicontinuous $Ia\bar{3}d$/gyroid* phase occurred over $0.36 \leq f_{PI} \leq 0.39$, for degrees of segregation ($\chi N$) ranging from about 20 at the ODT to 27. It

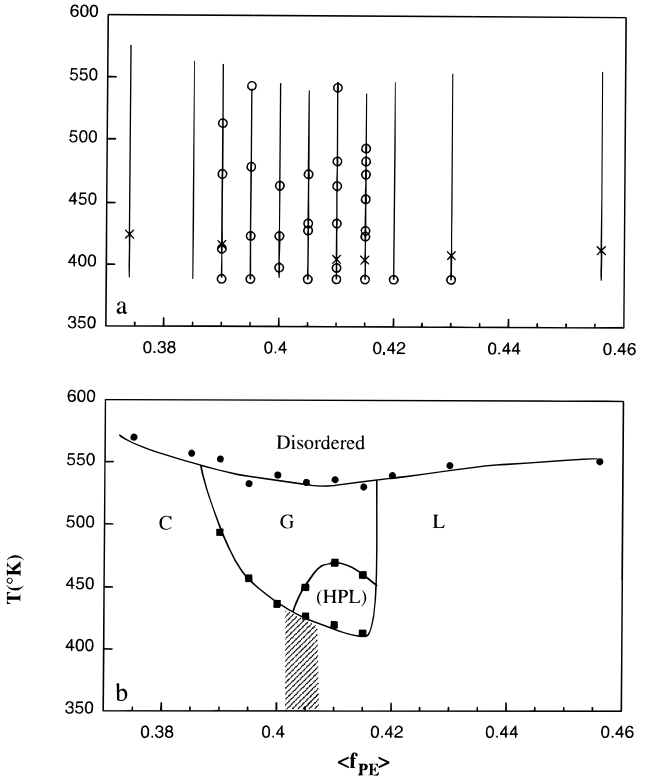


**Figure 17.** (a) Summary of experiments performed with the diblock copolymer blends ($f_{PE}$ = 0.37 and $f_{PE}$ = 0.46) as a function of temperature and the minority block volume fraction. Vertical lines identify the temperature range for DMS measurements; ○ symbols indicate SANS on sheared specimens; × symbols identify annealing temperature prior to liquid nitrogen quenching for TEM analysis. (b) A "phase diagram" for PE−PEE diblock coplymer blends constructed based on the DMS, SANS, and TEM results. ● and ■ indicate OOT and ODT temperatures, respectively, determined from isochronal $G'(T)$ measurements (see Figure 10). The C, G, and L morphologies have been identified based on SANS and TEM results while the HPL state is a tentative assignment. Solid curves have been drawn following the apparent trends associated with the OOTs and ODTs. A morphology could not be assigned to the shaded region, although DMS measurements indicate a low-symmetry microstructure, e.g., L, C, or a two phase (L + C) state.

was bounded by cylinders, lamellae, and HPL. The present work indicates that the $Ia\bar{3}d$/gyroid* phase appears in single-component PE−PEE specimens for $0.37 < f_{PE} < 0.43$; the analogous composition range for the blends is $0.390 < \langle f_{PE} \rangle < 0.420$. Any shift in the location of the bicontinuous phase between PI−PS and PE−PEE might be attributable to the difference in conformational asymmetry as discussed elsewhere;[14] $\epsilon_{PI-PS} \sim 1.5$, while $\epsilon_{PE-PEE} \sim 2.5$. Qualitatively similar results have also been obtained from polystyrene−poly(2-vinylpyridine) (PS−PVP)[27] and poly(ethylenepropylene)−poly(ethylethylene) (PEP−PEE)[14] diblock copolymers and blends, leading us to conclude that the occurrence of the bicontinuous $Ia\bar{3}d$/gyroid* phase is a universal feature of these materials. One notable exception is the poly(ethylene)−poly(ethylenepropylene) (PE−PEP) system, where an extensive investigation of pure and blended diblocks has failed to uncover a bicontinuous morphology.[14,39] None of our experiments have revealed any evidence of the ordered bicontinuous double diamond (OBDD) microstructure although the $Ia\bar{3}d$/gyroid* phase has been observed in all but one of the diblock copolymer systems we have examined.[3,6,7,10,14,27] A recent reevaluation of two of the original OBDD starblock materials has led to a

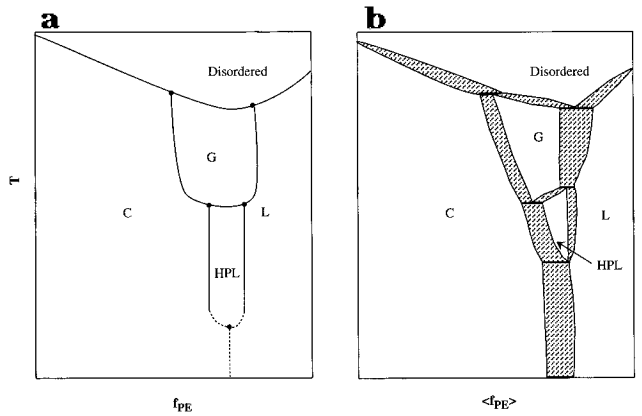


**Figure 18.** Schematic illustration of phase topology in (a) pure PE−PEE diblock copolymers and (b) diblock copolymer mixtures. These diagrams are qualitatively consistent with the results presented here and our earlier results for PI−PS diblocks.[3] Triple points are indicated by the symbol ●. The two-component phase diagram (b) contains two phase regions (shaded) and constant-temperature three-phase lines. This depiction is one of several possible constructions that would be consistent with the observed phase behavior (Figure 17).

reassignment of the $Ia\bar{3}d$/gyroid* morphology.[10] However, given the frequent occurrence of this bicontinuous microstructure in certain highly solvated lyotropic liquid crystal systems,[36] we cannot rule out the possibility that it may be found in other materials.

The blend phase diagram identified in Figure 17b cannot be correct in detail. Because of the extra degree of freedom associated with two components (versus one), the order−order phase boundaries will generally be biphasic, and the triple points that appear in the pure block copolymer system will be transformed into three-phase lines. A schematic comparison of the phase behavior we find for pure diblocks[3,14,27] with one (of several) possible blend phase diagram in the vicinity of the L−C transition near the ODT is presented in Figure 18. The blend illustration resembles what is commonly found in binary alloys of elements and compounds in the proximity of a homogeneous liquid phase.[40−42] However, we have not actually identified biphasic or triphasic regions in the PE−PEE blends discussed here. Moreover, mean-field theory[43] predicts that the two-phase windows may be extremely small for these mixtures.[27] Of course, this situation will change as the disparity in molecular weight and composition between components increases. In a separate paper[44] we will show that the location of the G phase shifts to $0.31 \lesssim \langle f_{PE} \rangle \lesssim 0.34$ when the $f_{PE} = 0.25$ and $f_{PE} = 0.49$ samples are blended. Recent theory[45] suggests that when $\Delta f$ is made sufficiently large, macroscopic phase separation will occur; clearly when $\Delta f = 1$ (i.e., homopolymer mixtures), order is completely lost.

Finally, we return to the dynamic mechanical spectra presented in Figures 4 and 11. Obviously, the viscoelastic properties of ordered block copolymers are dependent on microstructure type at frequencies lower than the inverse molecular relaxation (i.e., reptation) time, $\omega < \tau^{-1}$. The general trend that is observed is an increase in $G'$ (and $G''$) with increasing microstructure connectivity. Thus, the bicontinuous microstructure is more elastic than the monocontinuous HPL, which is more elastic than the cylindrical or lamellar states. However, this rationalization fails to account for the properties of the BCC sphere material, an "unconnected" morphology, which are essentially indistinguishable from those of the bicontinuous one. Apparently, it is the cubic (and possibly body-centered cubic) symmetry,

not the microstructural connectivity, that is most responsible for the development of a highly elastic linear dynamic mechanical response. (This result suggests that a cubic−cubic order−order transition may not be evident in a DMS experiment.) A feature common to both cubic phases is a crossover at low frequencies to a loss-dominated complex modulus. Although we lack a firm understanding of this behavior, we note that it is inconsistent with the behavior of a permanent network-like system (e.g., a cross-linked gel) or a true elastic solid (e.g., a metal or ceramic). Instead, this characteristic may be related to the proximity of these materials to the ODT, where fluctuations influence both thermodynamic and dynamic properties.[31,33,46] In the $Ia\bar{3}d$/gyroid* phase we associate such fluctuations with the local disruption of 3-dimensional order; this could result in the long-time dissipation of an applied stress. The picture is somewhat easier to envision in the case of BCC spheres. Here, fluctuations would correspond to isotropically distributed lattice defects, such as vacancies, that would increase in density as the ODT is approached. This situation is well documented in atomic crystals, although the weak first-order character of the order−disorder transition in block copolymers[28,46] would probably increase the number of such defects. We suspect that the effects of fluctuations are influenced by the microstructure symmetry, which may explain why $G''(\omega)$ and $G''(\omega)$ are so similar for the spherical and bicontinuous phases. This interesting aspect of block copolymer dynamics will be further examined in future publications. Here we note that such a fluctuation picture complements what has been demonstrated on the disordered side of the ODT. There, both small-angle scattering[20,46] and rheology[33] experiments have conclusively confirmed the fluctuation-induced weak first-order character of the ODT. That the bicontinuous $Ia\bar{3}d$ phase only occurs near the ODT is consistent with the notion that fluctuations influence (and perhaps stabilize) this microstructure.[6,14]

**Acknowledgment.** Work at the University of Minnesota was supported by an AFOSR grant (AF/F49620-93-1-0182) and the Center for Interfacial Engineering, an NSF-sponsored Engineering Research Center. F.S.B. and K.A. also benefited from a NATO travel grant. Work at Princeton University was supported by the U.S. Department of Energy (DE-FG02-87ER60522) and the National Science Foundation Materials Research Group (DMR-92-23966) and Materials Research Science and Engineering Center (DMR-94-00362).

## References and Notes

(1) Hamley, I. W.; Koppi, K. A.; Rosedale, J. H.; Bates, F. S.; Almdal, K.; Mortensen, K. *Macromolecules* **1993**, *26*, 5959.
(2) Hamley, I. W.; Gehlsen, M. D.; Khandpur, A. K.; Koppi, K. A.; Rosedale, J. H.; Schulz, M. F.; Bates, F. S.; Almdal, K.; Mortensen, K. *J. Phys. II (Fr.)* **1995**, *4*, 2161.
(3) Förster, S.; Khandpur, A. K.; Zhao, J.; Bates, F. S.; Hamley, I. W.; Ryan, A. J.; Bras, W. *Macromolecules* **1994**, *27*, 6922.
(4) Disko, M. M.; Liang, K. S.; Behal, S. K.; Roe, R. J.; Jeon, K. J. *Macromolecules* **1993**, *26*, 2783.
(5) Spontak, R. J.; Smith, S. D.; Ashraf, A. *Macromolecules* **1993**, *26*, 956; *Polym. Commun.* **1993**, *34*, 2233.
(6) Schulz, M. F.; Bates, F. S.; Almdal, K.; Mortensen, K. *Phys. Rev. Lett.* **1994**, *73*, 86.
(7) Hajduk, D. A.; Harper, P. E.; Gruner, S. M.; Honeker, C. C.; Kim, G.; Thomas, E. L.; Fetters, L. J. *Macromolecules* **1994**, *27*, 4063.
(8) Hasegawa, H.; Tanaka, H.; Yamasaki, K.; Hashimoto, T. *Macromolecules* **1987**, *20*, 1651.
(9) Thomas, E. L.; Alward, D. B.; Kinning, D. J.; Martin, D. C.; Handlin, D. L.; Fetters, L. J. *Macromolecules* **1986**, *19*, 2197.
(10) Hajduk, D. A.; Harper, P. E.; Gruner, S. M.; Honeker, C. C.; Thomas, E. L.; Fetters, L. J. *Macromolecules* **1995**, *28*, 2570.
(11) Matsushita, Y.; Tamura, M.; Noda, I. *Macromolecules* **1994**, *27*, 3680.
(12) Aushra, C.; Stadler, R. *Macromolecules* **1993**, *26*, 2171.
(13) Floudas, G.; Hadjichristidis, N.; Iatrou, H.; Pakula, T.; Fischer, E. W. *Macromolecules* **1994**, *27*, 7735.
(14) Bates, F. S.; Schulz, M. F.; Khandpur, A. K.; Förster, S.; Rosedale, J. H.; Almdal, K.; Mortensen, K. *Faraday Discuss. Chem. Soc.* **1994**, *98*, 7.
(15) Hashimoto, T.; Koizumi, S.; Hasegawa, H. *Macromolecules* **1994**, *27*, 1562.
(16) Turner, D. C.; Gruner, S. M.; Huang, J. S. *Biochemistry* **1992**, *31*, 1356.
(17) Hajduk, D. A.; Gruner, S. M.; Rangarajan, P.; Register, R. A.; Fetters, L. J.; Honeker, C.; Albalak, R. J.; Thomas, E. L. *Macromolecules* **1994**, *27*, 490.
(18) Oonk, H. A. J. *Phase Theory*; Elsevier: New York, 1981.
(19) Barrett, C. R.; Nix, W. D.; Tetelman, A. S. *The Principles of Engineering Materials*; Prentice-Hall: Englewood Cliffs, NJ, 1973.
(20) Rosedale, J. H.; Bates, F. S.; Almdal, K.; Mortensen, K.; Wignall, G. D. *Macromolecules* **1995**, *28*, 1429.
(21) Khandpur, A.; Macosko, C. W.; Bates, F. S. *J. Polym. Sci., Polym. Phys.* **1995**, *33*, 247.
(22) Bates, F. S.; Rosedale, J. H.; Bair, H. E.; Russell, T. P. *Macromolecules* **1989**, *22*, 2557.
(23) Fetters, J.; Lohse, D. J.; Richter, D.; Witten, T. A.; Zirkl, A. *Macromolecules* **1994**, *27*, 4639.
(24) Koppi, K. A.; Tirrell, M.; Bates, F. S.; Almdal, K.; Mortensen, K. *J. Rheol.* **1994**, *38*, 999.
(25) Tate, M. W.; Eikenberry, E.; Gruner, S. M., in preparation.
(26) Tepe, T.; Schulz, M. F.; Zhao, J.; Tirrell, M.; Bates, F. S.; Mortensen, K.; Almdal, K. *Macromolecules* **1995**, *28*, 3008.
(27) Schulz, M. F.; Khandpur, A. K.; Matsen, M.; Bates, F. S.; Almdal, K.; Mortensen, K.; Hajduk, D. A.; Gruner, S. M., in preparation.
(28) Almdal, K.; Bates, F. S.; Mortensen, K. *J. Chem. Phys.* **1992**, *96*, 9122.
(29) Khandpur, A. K.; Förster, S.; Bates, F. S.; Hamley, I. W.; Ryan, A.; Bras, W.; Almdal, K.; Mortensen, K. *Macromolecules* **1995**, *28*, 8796.
(30) Almdal, K.; Mortensen, K.; Bates, F. S., in preparation.
(31) Koppi, K. A.; Tirrell, M.; Bates, F. S. *Phys. Rev. Lett.* **1993**, *70*, 1449.
(32) Bates, F. S.; Koppi, K. A.; Tirrell, M.; Almdal, K.; Mortensen, K. *Macromolecules* **1994**, *27*, 5934.
(33) Rosedale, J. H.; Bates, F. S. *Macromolecules* **1990**, *23*, 2329.
(34) Winey, K. I.; Patel, S. S.; Larson, R. G.; Watanabe, H. *Macromolecules* **1993**, *26*, 2542.
(35) Koppi, K. A.; Tirrell, M.; Bates, F. S.; Almdal, K.; Colby, R. H. *J. Phys. II (Fr.)* **1992**, *2*, 1941.
(36) Seddon, J. M. *Biophys. Acta* **1990**, *41*, 525.
(37) Clerc, M.; Levelut, A. M.; Sadoc, J. F. *J. Phys. II (Fr.)* **1991**, *1*, 1263.
(38) Almdal, K.; Mortensen, K.; Bates, F. S., in preparation.
(39) Bates, F. S.; Rosedale, J. H.; Zhao, J.; Almdal, K.; Mortensen, K., in preparation.
(40) Oonk, H. A. J. *Phase Theory*; Elsevier: New York, 1981.
(41) Barrett, C. R.; Nix, W. D.; Tetelman, A. S. *The Principles of Engineering Materials*; Prentice-Hall: Englewood Cliffs, NJ, 1973.
(42) Levin, E. M.; Robbins, C. R.; McMurdie, H. F. *Phase Diagrams for Ceramists*; American Ceramic Society: Columbus, OH, 1964.
(43) Matsen, M. W.; Schick, M. *Phys. Rev. Lett.* **1994**, *72*, 2660.
(44) Zhao, J.; Majumdar, B.; Bates, F. S.; Almdal, K.; Mortensen, K., in preparation.
(45) Fredrickson, G. H., unpublished results.
(46) Bates, F. S.; Rosedale, J. H.; Fredrickson, G. H.; Glinka, C. J. *Phys. Rev. Lett.* **1988**, *61*, 2229. Bates, F. S.; Rosedale, J. H.; Fredrickson, G. H. *J. Chem. Phys.* **1990**, *92*, 6255.

MA9507251